Journal of Medicinal Chemistry

ARTICLE

pubs.acs.org/jmc

Structure-Based Design of Short Peptide Ligands Binding onto the *E. coli* Processivity Ring

Philippe Wolff,[■,†] Vincent Oliéric,[■,‡] Jean Paul Briand,[§] Olivier Chaloin,[§] Annick Dejaegere,[∥] Philippe Dumas,[†] Eric Ennifar,[†] Gilles Guichard,[⊥] Jérôme Wagner,[△,#] and Dominique Y. Burnouf[*,△,†]

[†]Architecture et Réactivité de l'ARN, Université de Strasbourg, Institut de Biologie Moléculaire et Cellulaire, 15 rue René Descartes, 67084, Strasbourg cedex, France

[‡]Swiss Light Source (SLS), Paul-Scherrer-Institute (PSI), Villigen, Switzerland

[§]CNRS, Institut de Biologie Moléculaire et Cellulaire, Immunologie et Chime Thérapeutiques, 15 rue René Descartes, 67084, Strasbourg cedex, France

[∥]IGBMC, Département de Biologie Structurale et Génomique, 1 rue Laurent Fries, BP10142, 67404 Illkirch, France

[⊥]Institut Européen de Chimie et Biologie, Université de Bordeaux-CNRS UMR 5248, CBMN, 2, rue Robert Escarpit, 33607 Pessac, France

[#]CNRS UMR7242, ESBS, Université de Strasbourg, BP 10413, 67412 Strasbourg Cedex, France

Supporting Information

ABSTRACT: The multimeric DNA sliding clamps confer high processivity to replicative DNA polymerases and are also binding platforms for various enzymes involved in DNA metabolism. These enzymes interact with the clamp through a small peptide that binds into a hydrophobic pocket which is a potential target for the development of new antibacterial compounds. Starting from a generic heptapeptide, we used a structure-based strategy to improve the design of new peptide ligands. Chemical modifications at specific residues result in a dramatic increase of the interaction as measured by SPR and ITC. The affinity of our best hits was improved by 2 orders of magnitude as compared to the natural ligand, reaching 10^{-8} M range. The molecular basis of the interactions was analyzed by solving the co-crystal structures of the most relevant peptides bound to the clamp and reveals how chemical modifications establish new contacts and contributes to an increased affinity of the ligand.

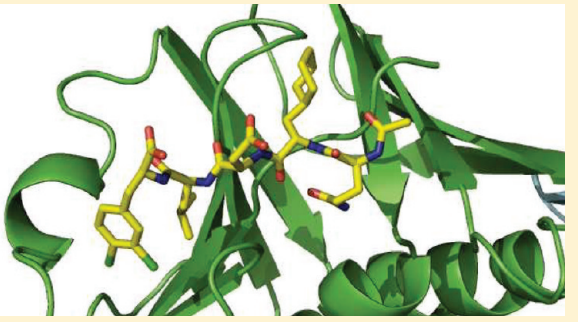

■ INTRODUCTION

In all three domains of life, multicomponent complexes, the so-called replisomes, have evolved to ensure the faithful replication of chromosomal DNA. One central protein of these complexes forms a ring that encircles and slides along the double-stranded DNA.[1,2] A physical interaction between the clamp and the chromosomal replicase confers a high processivity to the enzyme.[3] In bacteria, the processivity factor, also referred to as the β clamp (hereafter named β), is a homodimer, which results from the head-to-tail association of two monomers, each of them being shaped in three globular subdomains.[1] In eukaryotes and archae, the β homologue factor, PCNA (for proliferating cell nuclear antigen), is a homotrimer with each monomer organized into two subdomains.[2,4]

Besides their role as processivity factors for chromosomal replicases, β and PCNA clamps also participate in various protein−protein interactions. They notably act as landing platforms for factors involved in DNA metabolism and cell cycle regulation,[5] particularly DNA polymerases involved in translesion synthesis,[6,7] and factors promoting DNA repair.[8−10] All these factors possess a small conserved peptide sequence, which binds into a hydrophobic pocket located on one side of the clamp. It is noteworthy that these pockets differ significantly between bacterial and eukaryotic clamps. A bioinformatics analysis performed on putative β partners led to defining the bacterial consensus binding peptide QL[S/D]LF.[10] The absolute requirement of the interacting peptide for β clamp partners binding has been further demonstrated biochemically and physiologically.[11−14] Finally, the interaction between the clamp and the peptide of different β binding proteins has been structurally characterized.[15−18] The peptide binding site is formed by a deep leucine-rich hydrophobic pocket (subsite 1) located between subdomains two and three of the β monomer and connected via a groove to a second subsite (subsite 2) located in subdomain 3[17] (Figure 1C). An additional interaction has also been observed in the case of

Received: March 18, 2011
Published: May 30, 2011

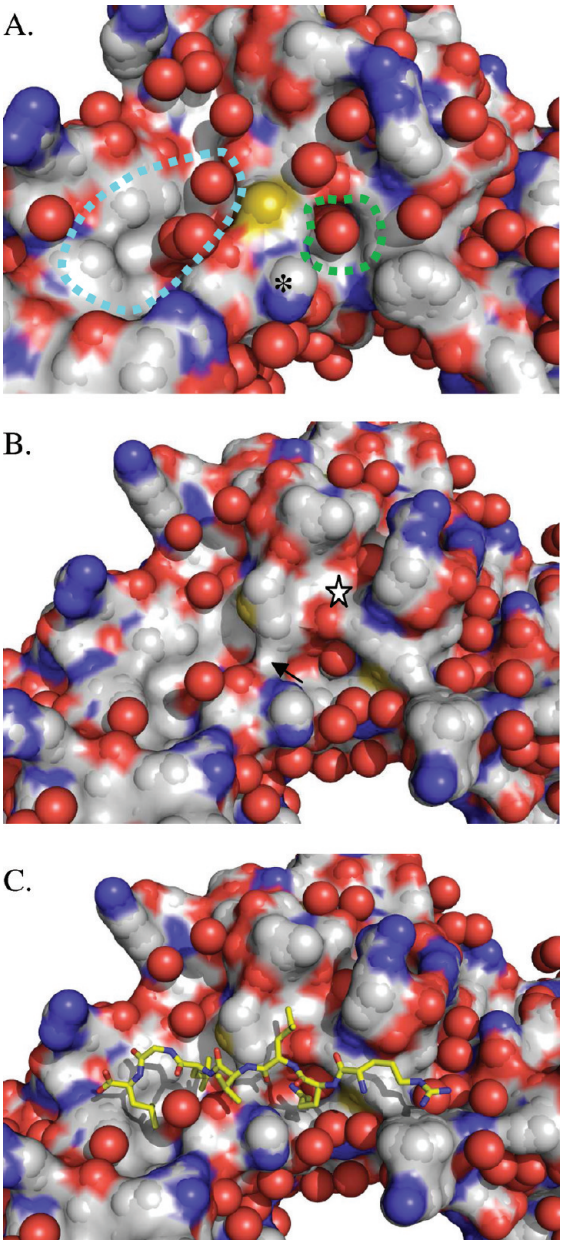

Figure 1. Representations of the ligand binding pocket of the β clamp of *E. coli*, from the co-crystal structure of β with the C-terminal peptide of the *E. coli* DNA polymerase IV ($R_1Q_2L_3V_4L_5G_6L_7$) (PDB code 1OK7). (A) unbound pocket: the M_{362} (yellow) residue is located close to the H_{175} β residue (*) and obstructs the path between subsite 1 (blue dots area) and subsite 2 (green dots area). Water molecules are represented as red balls. (B) bound pocket. The peptide has been removed. The movement of residue M_{362} opens a cleft (dark arrow) which connects subsite 1 and subsite 2 and where the V_4 peptide residue interacts (see C). Water molecules are displaced, as compared to A, so that the peptide can fit into subsite 1. Note the opening of the platform (white star) between M_{362} and R_{365} where the L_3 peptide residue will be located. (C) Same as B but with the peptide P1 bound into the pocket.

the polymerase Pol IV, between the little finger domain of the enzyme and the edge of the β clamp.[16]

In both prokaryotes and eucaryotes, the peptide-mediated interactions between DNA polymerases and the replicative clamps are absolutely required to ensure successful DNA

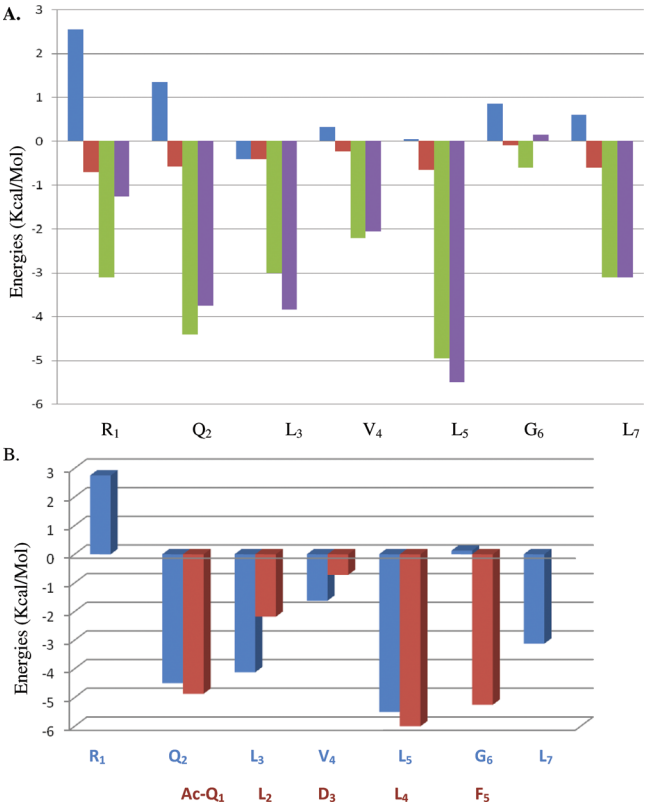

Figure 2. (A) Energetic contributions (kcal/mol) of each peptide residue ($R_1Q_2L_3V_4L_5G_6L_7$) for the interaction within the β binding pocket (PDB 1OK7). Blue: electrostatic contribution. Red: solvent accessible surface contribution. Green: van der Waals contribution. Magenta: total contribution. (B) Single residue contribution (kcal/mol) to the peptide binding. Native peptide P1 of *E. coli* DNA polymerase IV, from the structure 1OK7, is in blue. The pentapeptide P6 is in red (PDB 3Q4J).

replication and ultimately cell survival. As a consequence, the interacting pockets are potential targets for the development of new antibacterial or anticancer drugs, respectively.

In a recent report, a chemical compound was identified from a library and shown to bind into the leucine-rich subdomain of the *E. coli* β clamp interacting pocket with an affinity of 10^{-5} M.[18] In the present work, we have used a structure-based strategy to design short peptides with improved affinities for the β clamp interacting pocket. These peptides are potential leads for new antibiotic compounds. The first step of our approach was to decipher the molecular basis of the interaction of the natural ligand in the binding pocket. Using these data, we designed a first peptide (P6) that was further modified to improve its affinity. Several biophysical and biochemical methods were used to measure the strength of the interaction and to characterize the structure of the most efficient complexes formed. As a result, the binding efficiency of the modified ligand was improved by 2 orders of magnitude, reaching 10^{-8} M range.

RESULTS

Structure and Energetics of the Binding Pocket. We have previously solved the structure of a complex formed between the *E. coli* β clamp and the 16-residue-long C-terminal peptide of the *E. coli* DNA polymerase IV (PDB code 1OK7).[17] A first part of the present work aimed at unraveling the molecular basis of the

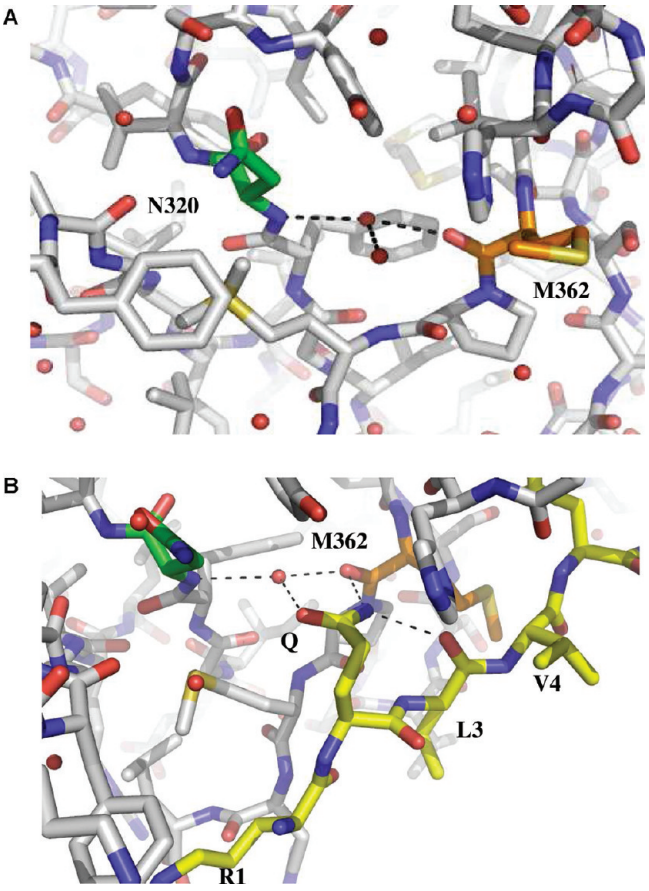

Figure 3. Detailed connectivities between β residues N_{320} (green) and M_{362} (orange) in subsite 2 of the binding pocket, in absence (A) or presence (B) of the peptide (yellow). Red balls represent water molecules. From PDB structure 1OK7.

peptide−pocket interactions. We used molecular modeling approaches to determine the contribution of each residue of the last seven amino acids of the C-terminal part of Pol IV ($R_1Q_2L_3V_4L_5G_6L_7$) to the overall interaction (Figure 2A), using free energy decomposition (see Experimental Section). For each amino acid, the van der Waals, electrostatic, and hydrophobic solvation contributions to binding have been calculated. Stabilizing interactions between β and the peptide are essentially van der Waals contacts (see Figure 2A). Electrostatic contributions are poor, due to compensation between the protein−peptide interaction and the peptide desolvation cost. Hydrophobic solvation contributions are favorable but of lesser magnitude. The net contributions of residues Q_2, L_3, L_5, and L_7 are predominant to the overall interaction (Figure 2B). G_6 has no contribution, while V_4 which is oriented toward the solvent poorly contributes to the interaction.

Due to the good resolution, we could also analyze the position of water molecules in the free and bound pockets of the 1OK7 structure. In the absence of peptide, four water molecules are located in subsite 1. Upon peptide binding, one is eliminated and one is repositioned close to the T_{142} and Y_{154} residues, allowing the L_5-G_6-L_7 tripeptide to bind into the hydrophobic subsite 1 (Figure 1AB). The two water molecules located on the platform in the apo monomer are dislodged upon peptide binding, thus making room for the peptide L_3 residue to bind (Figure 1BC). Finally, two water molecules are deeply inserted into the empty

Table 1. Influence of the C-Terminal Tripeptide Sequence and Effect of Site-Specific Modifications on the Interaction of Peptide with the *E. coli* β Clamp[a]

#	sequence	IC_{50} (μM)	K_i (10^6 M^{-1})	ΔG (kcal/mol)
PolIV		0.29	4.7	−9.09
P1	RQLVLGL	8.85	0.15	−7.06
P2	RQLVLL	21.53	0.0063	−6.54
P3	RQLVLF	8.62	0.15	−7.04
P4	RQLVFL	256	Ø	Ø
P5	QLDLF	12.44	0.11	−6.87
P6	AcQLDLF	1.12	1.2	−8.22
P7	Ac Q ChaDLF	0.17	8.01	−9.42
P8	Ac Q hCha DLF	82.8	16.4	−5.74
P9	Ac Q Hol DLF	0.74	1.84	−8.54
P10	Ac Q NptGly DLF	0.99	1.36	−8.36
P11	Ac-Q Cha DL pMeF	0.26	8.43	−9.44
P12	Ac-Q Cha DL pClF	0.16	13.7	−9.73
P13	Ac-Q Cha DL pBrF	0.096	13.49	−9.71
P14	Ac-Q Cha DL diClF	0.077	17	−9.85

[a] As measured by SPR experiments. Ø: not determined. $K_i = (1 + K_A[\beta])/IC_{50}$. $\Delta G = -RT \ln K_i$. PolIV:*E. coli* DNA polymerase IV.

subsite 2. One of these two molecules interconnects the $N_\alpha H$ of N_{320} and the $C_\alpha{=}O$ of M_{362} (Figure 3) and is not exchanged with the solvent upon peptide binding, underlining its structural function. The second water molecule is replaced by the $C\delta{=}O$ of peptide Q_2 residue, while its δ-amino group establishes bounds with the $C\alpha{=}O$ of M_{362} and the $C\alpha{=}O$ of peptide residue L_2 (Figure 3B).

This initial analysis led us to design a minimal peptide binding sequence that we used as a starting point for ligand optimization. Because of the complex network of hydrogen bonds formed by the highly conserved Q residue in subsite 2, one cannot substitute this side chain without dramatically altering the interaction of the whole peptide. Alternatively, several other positions in the peptide sequence may be subjected to modifications that could increase its affinity to the β clamp. Following the structural and energetic analysis of the binding pocket (see Experimental Section), several peptides were synthesized (Table 1 and Supporting Information 1) and their binding efficiencies were analyzed by surface plasmon resonance (SPR). The dissociation constant of the P1 natural heptapeptide was measured to be 2.85 ($\pm$0.94) 10^{-7} M. As compared to the whole polymerase, this peptide binds 30-fold less efficiently to β (Table 1, compare P1 and PolIV), pinpointing the contribution of alternate regions of the enzyme to the interaction.[14,16,19] Removing the G residue of the terminal tripeptide (−LGL) results in a 2- to 3-fold decrease in interaction (Table 1, compare P1 and P2), while replacing the terminal tripeptide with the consensus LF dipeptide does not affect the affinity (Table 1, compare P1 and P3). However, a FL dipeptide totally impedes peptide binding (Table 1, P4). Substituting F for other aromatic residues (W,Y) at the C-terminal position does not contribute to any increased interaction (data not shown). In order to design the shortest peptide, we also removed the first (R_1) residue, which does not seem to contribute significantly to the binding (Table 1, P5, Figures 1 and 2),[17] and we replaced the V_4 by a D residue, as observed in the consensus sequence, in order to increase the solubility of the resulting pentapeptide P5 (QLDLF). Although its affinity to β is

low, it was increased by 10-fold upon acetylation (Table 1, compare P5 and P6), thus providing a good compromise between interaction efficiency and ligand size.

Crystal Structure of the P6-β Complex. The P6 peptide (AcQLDLF) co-crystallized with β in conditions similar to those previously described,[17] but the cell parameters lead to a V_M value of 7.8, which corresponds to the presence of 3 dimers per asymmetric unit (Supporting Information 2). This structure was solved by molecular replacement at 2.3 Å resolution, using our previously determined structure (PDB 1OK7). The superposition of main chain atoms of each monomer to the A monomer of this structure led to rmsd values ranging from 0.35 Å to 0.62 Å, underlining the close structural similarity of each monomer. Similarly, all six bound peptides adopt a similar conformation in all six hydrophobic pockets, as indicated by rmsd values ranging between 0.25 Å and 0.51 Å.

A free energy decomposition analysis (see Experimental Section for details) of this complex was performed (Figure 2B) and the most important interactions are similar to the initial complex 1OK7, as expected. The canonical sequence LF advantageously replaces the LGL sequence in C-terminal position of the peptide (Figure 2B). The P6 peptide acetyl group also forms two hydrogen bonds with the N_α of residues R_{365} and L_{366} of the β monomer which probably account for the 10-fold increase in stability of the P6 peptide as compared to P5 (Table 1). Despite its reduced size, the P6 peptide therefore has an increased affinity to the β-clamp with respect to the original peptide P1.

Design of Non-Natural Peptide Ligands with Increased Binding Affinity. P6 was further used as a lead to introduce modifications aimed at increasing the affinity of the ligand for the β clamp. Because the natural ligand binds to the pocket essentially through hydrophobic interactions, we tried to extend the network of such interactions. A first set of modifications concerned position 2, where the leucine residue was replaced by a cyclohexyl-L-alanyl group (Cha) (P7, Table 1). An initial modeling analysis, using programs MCSS and SEED, indicated that this modification provides a van der Waals energy contribution 2-fold higher than that with the natural L_3 residue, and is the most efficient group tested (data not shown). It also results in a 6-fold increase in the interaction, as measured by SPR (Table 1, compare P6 and P7). Attempts to increase the side chain length result in a drastic reduction of the affinity (Table 1, P8), while other modifications like homoleucyl (Hol) or neopentylglycyl (NptGly) did not yield any gain in affinity (Table 1, P9 and P10), probably indicating that the area available for an efficient interaction is limited. A second set of similar modifications was introduced at position L_4, but no increase in affinity was observed as compared to P7 (data not shown). Finally, several modifications were introduced on the terminal phenylalanine benzyl ring. The binding affinity was found to increase significantly with the size of the ring substituent (*p*-methyl < *p*-chloro < *p*-bromo < 3,4-dichloro). An IC_{50} value of 70 nM was measured for the 3,4-dichlorophenylalanine containing peptide (P14), which represent a 15-, 115-, and 4-fold increase as compared to P6, P1, and the full PolIV enzyme, respectively (Table 1).

The interaction of the various peptides with β were also evaluated using a polymerase competition assay where primer elongation performed by the polIV DNA polymerase is challenged by various concentrations of the peptides to be tested.[17] While the β independent activity of the polymerase is insensitive to the peptides, indicating that they have no direct effect on the enzyme activity, the β dependent elongation activity is differentially inhibited depending on the affinity of the peptide for its target (Figure 4). A quantitative analysis of the biochemical assays is available as Supporting Information 3. Although this approach is less sensitive than SPR, a good correlation is observed between the two methods (Figure 4).

Crystal Structure of the Modified Peptides-β Complexes. Peptides P12 and P14 were co-crystallized with β. The structures were solved by molecular replacement at 2.6 Å and 1.95 Å resolution, respectively, using the 1OK7 structure as a search model. As for the previous P6-β complex, both complexes crystallized in space group *P*1 but with one ring per asymmetric unit (Supporting Information 2). Each monomer of the rings binds a peptide, and both ligands adopt a similar configuration (rmsd = 0.70 Å and 0.78 Å for the peptide atoms of P12 and P14, respectively), indicating that the modified peptides essentially adopt the same conformation and location in the binding pocket. The Cha moiety is located at the same position as the L_3 residue of P6 but extends its interaction further within a hydrophobic pocket shaped by the P_{363}, V_{344}, M_{362}, and R_{365} β residues (Figure 5A) and interacts with the last three residues. These extra interactions probably account for the increased affinity of P7 as compared to P6 (Table 1). Additionally, the N_α of this modified residue interacts with the C_α=O of P_{363}. The *p*-chloro and 3,4-dichloro F residues of P12 and P14 are almost superimposed (Figure 5B) and interact with β residues T_{172}, L_{177}, and V_{247}. The chlorine atom in meta position in P14 establishes a halogen bond with the hydroxyl oxygen of T_{172}, with contact distance and angle in good agreement with previously published data (d = 3.17 Å and Θ = 148.71°).[20] In contrast, the para chlorine atoms of both P12 and P14 do not establish such an interaction because the distances between adjacent oxygen atoms of β residues are too large.

Thermodynamic Analysis of the Pseudo Peptide Interaction with β. ITC experiments were conducted on selected peptides in order to determine the thermodynamics parameters of their interaction with β (Table 2 and Supporting Information 4). Although the K_d values determined in these experimental conditions were slightly different from those obtained by SPR, the same tendency was observed for all peptides (Table 2). The largest differences are observed for low affinity peptides (P1, P3, P6), while for higher affinity peptides (P7, P11, P12, P13, and P14), both techniques yielded similar values. The introduction of modifications, Cha group in position 2 and *p*-methyl, *p*-chloro, and *p*-bromo groups on F_5, increases the affinity of the ligand, reaching, respectively, about 380, 100, 65, and 150 nM range, as compared to the 1−2 μM affinity of the reference natural peptide P1 (Table 2). A strong correlation is observed between ΔH and ΔS values (Supporting Information 4), which reflects an enthalpy−entropy compensatory effect, already observed in other systems.[21,22] This correlation accounts for the small ΔG variation among the various peptides (Supporting Information 4). As reported earlier,[23] this correlation suggests that the observed desolvation of the pocket upon ligand interaction plays a major role in the binding process.

The effect of the various modifications introduced in the peptides can be estimated from the $\Delta\Delta G$ values (see Table 3). The Cha moiety in position 2 contributes to the increased interaction by −0.66 kcal/mol as compared to the natural pentapeptide P6. While the introduction of a methyl substitution on the ring of the terminal phenylalanine residue is detrimental to the affinity (+0.25 kcal/mol), halogen modification

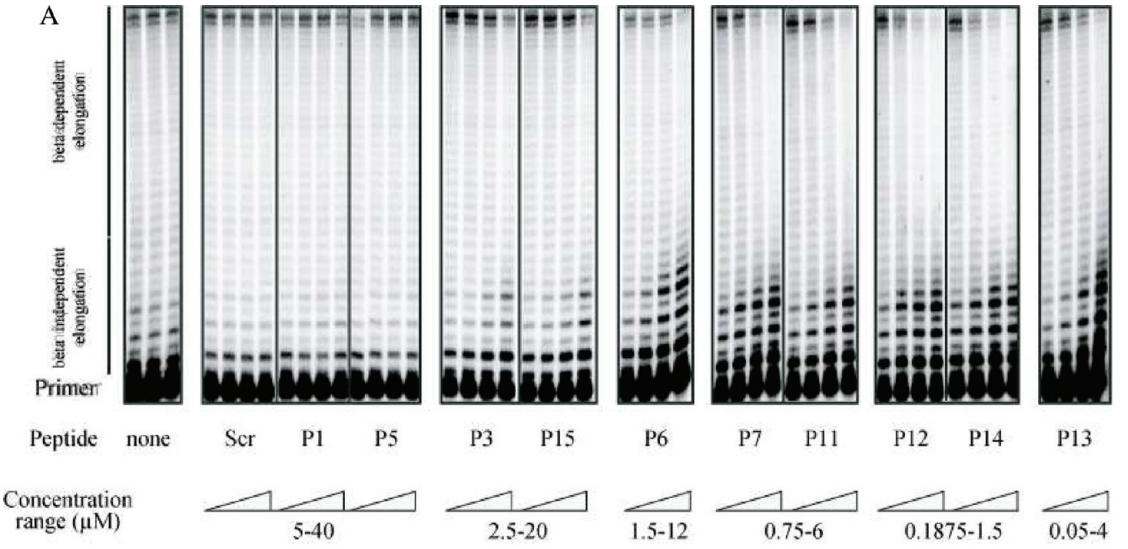

B

	P1	P5	P3	P15	P6	P7	P11	P12	P14	P13
IC50 Biochemical assay (μM)	nd	nd	7	6,7	4,5	2,8	2	0,3	0,125	0,25
IC50 SPR (μM)	8.85	12.44	8.62	1.91	1.12	0.17	0.26	0.16	0.077	0.096

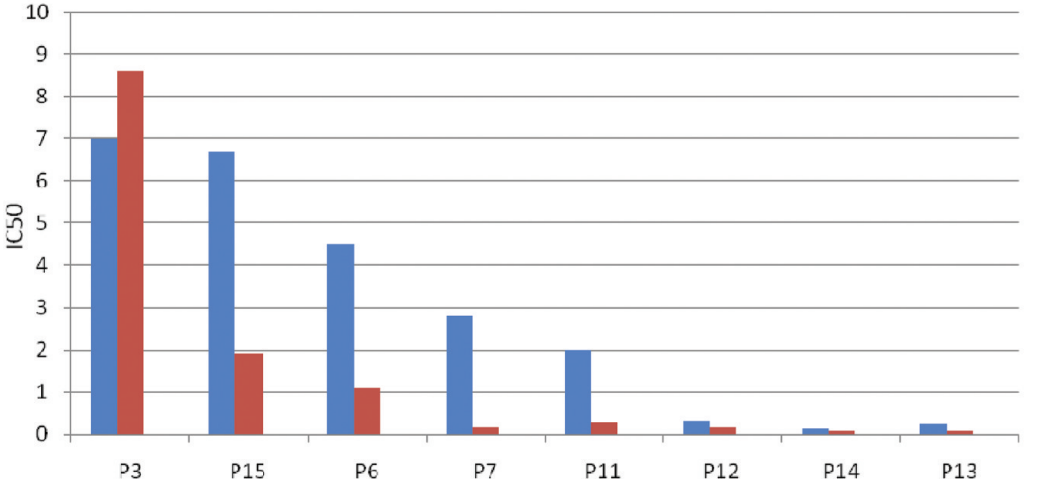

Figure 4. Polymerase competition assay. (A) The β dependent activity of PolIV DNA polymerase is challenged by increasing concentrations of various peptides (B) The table displays the IC_{50} determined for various peptides by the Pol IV based biochemical assay and the SPR assay. The histogram indicates that the same general trend is observed with both techniques despite a difference in sensitivity. Blue: biochemical assay. Red: SPR assay. P15 sequence is Ac-RQLVLF, Scr: scrambled peptide: Ac-ChaFQLD.

results in a progressive effect on ligand affinity (*p*-bromo < *p*-chloro < 3,4-dichloro). The chloro modification in the para position contributes for the main part to the increased affinity (−0.6 kcal/mol). This contribution can result partly from an increased hydrophobic character of the halogen modified F residue,[24] as well as from dehydration of both peptide and sub site 1[25] and reorganization of water molecules as observed by comparing free and bound β interacting pockets (Figure 1AB). In comparison, the second chlorine atom (meta position) in P14 only contributes for −0.2 kcal/mol and the para-bromo modification contribution to the binding energy is two times lower (−0.28 kcal/mol) than the corresponding para-chloro modification.

DISCUSSION

Fully Efficient β Binding Pocket Is Formed upon Ligand Binding. Many cellular factors involved in replication and genome integrity survey processes require a peptide-mediated interaction with the replisome sliding clamp in order to fulfill their function. This interaction has been structurally fully characterized in prokaryotes[16−18] and eucaryotes.[2,26] In our previously

dx.doi.org/10.1021/jm200311m |*J. Med. Chem.* 2011, 54, 4627–4637

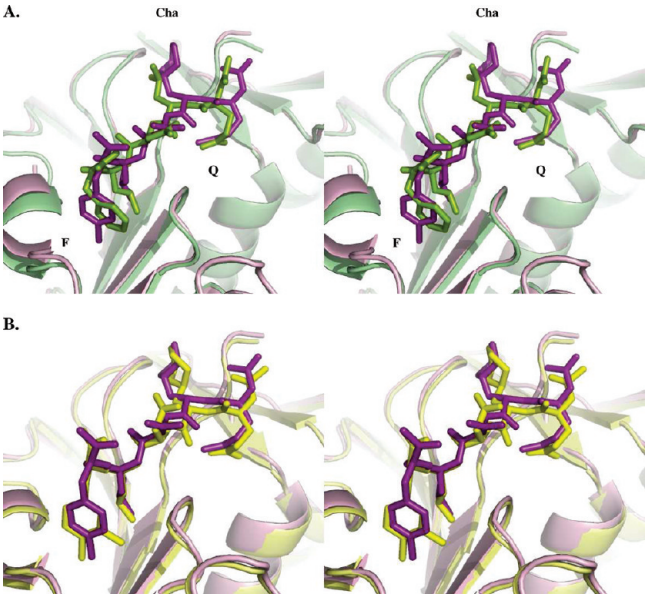

Figure 5. Superimposition of peptide-β complexes. (A) A P6-β complex (green, light green) is superimposed on P12-β complex (purple, pink) (rmsd: 0.95 Å). The first (Gln) and last (Phe) peptide residues are indicated. The Cha group of P12 peptide occupies the same position as the Leu_2 residue of P6. The chloro-modified Phe residue of P12 is tilted toward the bottom of subsite 1 as compared to the cognate residue of P6. (B) P14-β complex (yellow, lemon) is superimposed on P12-β complex (purple, pink) (rmsd: 0.56 Å). The chlorine atom in the meta position forms a halogen bond with the T172 residue.

published structure (1OK7), only one peptide binds to β, leaving one binding pocket free.[17] This provides the opportunity to compare the structure of a peptide-free versus a peptide-bound pocket and to gain insight into the dynamics of the pocket upon peptide binding. Although the general structures of the free or bound pockets are similar, as estimated by the C_α chain conformation (rmsd = 0.36 Å), the side chains of several residues undergo major movements (Figure 6), notably residues M_{362} and S_{346} side chains, which are displaced in a concerted way, and residue R_{365}. We presume that the concerted shift of M_{362} and S_{346} side chains is a structural marker for the presence of a peptide ligand in the binding pocket. In the absence of the ligand, these residues adopt a so-called close conformation where the M_{362} side chain is oriented toward residue H_{175} and separates subsite 1 and subsite 2 (PDB IDs 2POL, 1MMI, and 1OK7 (monomer A)) (Figure 6). Alternatively, in all β bound structures (1UNN, 1OK7 (monomer B), 3D1E, 3D1F), the residues are shifted by 180° in an open conformation, allowing the opening of a cleft joining the two subsites (Figure 1BC). One exception is found in the structure of β co-crystallized with the Pol II peptide (3D1E) where no ligand is observed in monomer B, although the two residues adopt an open conformation.[18] This may result from a partial occupancy of the pocket, making the detection of the peptide difficult.

Residue R_{365} is also shifted by an angle of 46° toward residue L_{366}, triggering the opening of a platform shaped by R_{365}, P_{363}, M_{362}, and V_{344}, where the L_3 residue of the peptide locates (Figure 1BC). The global dynamic of this structural modification has been modeled (Supporting Information 5), showing that, as the ligand binds into the pocket, a groove forms that joins subsite 1 and subsite 2, in which the extended peptide can adapt.

The correlation between side chain orientations and the presence of a peptide in the binding pocket suggests that these two side chains might play a strategic function in the ligand binding process. The pocket could adopt two configurations: a closed configuration where the M_{362} side chains lies in the path between the two subsites of the pocket, thus impeding the formation of an efficient binding site (Figure 1A). Alternatively, an open configuration where the M_{362} side chains shift by about 180°, allowing ligand binding into the groove that joins the two subsites, as well as the opening of the platform, so that the peptide establishes optimal interactions. At present, it is not known if the fully efficient binding pocket is readily available at the surface of the protein or is structured by the binding of a specific ligand, according to a bona fide induced fit model. Previous observations for a ligand binding site on the cytokine IL-2[27] reveal that a portion of the binding site is adaptive and can form a hydrophobic channel upon ligand binding. A similar adaptive process could occur for the β binding pocket and would ensure the binding specificity of ligand proteins. Although the details of the dynamic process of this binding site formation are not known yet, this observation is likely to have major implications for the design of high-affinity ligands.

Structure-Based Design of High-Affinity Ligands. We have studied the interaction of various peptides with the *E. coli* processivity clamp. Starting from the natural sequence of the Pol IV DNA polymerase interacting peptide (P1, RQLVLGL), we have sequentially modified the peptide in order to increase its interaction strength and concomitantly to limit its size. The affinities were measured by biochemical assays, SPR and ITC, and despite a difference in sensitivity of these various techniques, the relative affinities of the peptides were similar. From the P1-β complex (PDB 1OK7), a minimal acetylated peptide (P6, AcQLDLF) was first delineated and found to bind about eight times more tightly than P1. Then, we used the crystallographic structure of the P1-β and P6-β complexes together with modeling information to guide modifications at specific positions (corresponding to residues L_2 and F_5 of P6, AcQLDLF), resulting in a dramatic increase of the modified peptide affinity to the β interacting pocket. This gain essentially results from an increase in hydrophobic interactions. A first improvement was achieved by the introduction of a cyclohexylalanyl residue at the P6-L2 position. Although position 2 does not correspond to a major binding pocket on the β-clamp, the simple modification to a cyclohexylalanyl residue (P7) improved the affinity by a factor of 6 with respect to the P6 peptide (Table 1), indicating that shallow secondary sites can still prove useful in a global optimization scheme.

The other interesting gain was achieved by the addition of halogen atoms on the benzyl ring of the F residue. Interestingly, the chlorine atom, when introduced at the meta position, forms a halogen bond that further strengthens the interaction. P14, which combines both the Cha and a 3,4-dichloro phenylalanine residue, displays the highest affinity, around 60 ($\pm$10) nM as measured by ITC, which represents a 10- to 15-fold increase in binding as compared to P6 and a 4-fold increase as compared to the whole PolIV DNA polymerase. The double F ring substitution contributes for $-$0.8 kcal/mol to the overall interaction. The para-chloro substitution provides most of the contribution to the binding, while the meta-chloro, involved in a halogen bond, only contributes to one-fourth of the total free energy.

Interestingly, halogen-substituted aromatic ligands were also recently independently identified for the β-clamp using a chemical

Table 2. ITC Experiments on Selected β Binding Peptides[a]

β (μM)	pep (μM)	name	N	K_d (nM)	IC_{50} SPR (nM)	ΔH (cal/mol)	ΔS (cal/mol/deg)	ΔG (kcal/mol)
30	400	P1	1.33	1579	8850	−4087	12.8	−7.9
		RQLVLGL	1.31	2012		−5500	7.6	−7.7
30	400	P3	1.54	2816	8620	−5769	6.05	−7.5
		RQLVLF	1.45	2320		−5699	6.6	−7.6
30	400	P6	1.11	820	1120	-1.13×10^4	−10.4	−8.1
		AcQLDLF	1.14	613		-1.11×10^4	−9.08	−8.3
30	400	P7	0.74	246	170	-2.13×10^4	−41.2	−8.9
		AcQChaDLF	0.76	222		-2.05×10^4	−38.5	−8.9
20	400	P11	0.95	401	260	-1.48×10^4	−20.4	−8.6
		AcQChaDLpMeF	0.95	362		-1.44×10^4	−19.0	−8.6
20	400	P12	1.02	89	160	-1.5×10^4	−18.1	−9.6
		AcQChaDLpClF	1.06	122		-1.43×10^4	−16.3	−9.4
20	400	P13	0.85	136	96	-1.81×10^4	−29.3	−9.3
		AcQChaDLpBrF	0.83	167		-1.52×10^4	−20.2	−9.1
20	400	P14	0.91	73	77	-1.89×10^4	−30.8	−9.6
		AcQChaDLdiClF	0.90	55		-1.81×10^4	−27.6	−9.8

[a] $\Delta G = \Delta H - T\Delta S$. All experiments were performed at 25 °C. Results from SPR experiments (IC_{50}) are added for comparison purposes. N: number of binding sites per β monomer.

Table 3. Effects of Modifications Introduced in the Various Pentapeptides[a]

ΔGi/ΔGj	P6/P7	P7/P11	P7/P12	P7/P14	P7/P13	P11/P12	P11/P14	P11/P13	P12/P14	P13/P12	P13/P14
Compared residues	L/Cha	F/pMeF	F/pClF	F/diClF	F: pBrF	pMeF/pClF	pMeF/diClF	pMeF/pBrF	pClF/diClF	pBrF/pClF	pBrF/diClF
ΔΔG (kcal/mol)	−0.66	+0.25	−0.6	−0.8	−0.28	−0.85	−1.05	−0.53	−0.2	−0.32	−0.52

[a] Measured from the ΔΔG values extracted from ITC experiments data. The P6 sequence (AcQLDLF) is chosen as a reference. $\Delta\Delta G = \Delta Gj - \Delta Gi$.

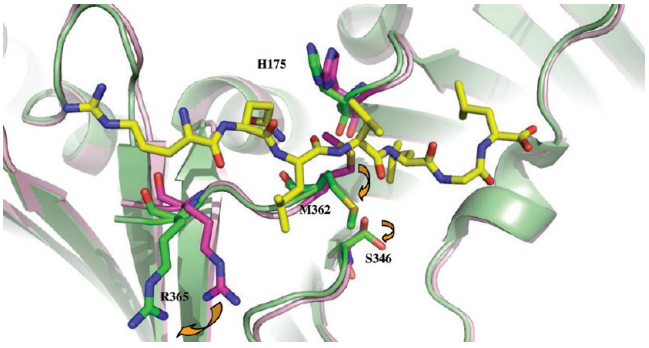

Figure 6. Superposition of the peptide-free (pink) and peptide-bound (green) interacting pockets of 1OK7 structure. In the absence of peptide, the M_{362} side chain (pink) is located close to the H_{175} residue (closed conformation) and separates subsite 1 and subsite 2. When the peptide is bound, the M_{362} side chain (green) is displaced away from the H_{175} (open conformation) allowing the opening of a cleft in which the peptide can bind. Residue R_{365} is also shifted upon peptide binding, triggering the opening of a small platform where the peptide L_3 residue locates.

library screening strategy. A compound, named RU67, was identified as a β ligand inhibiting the *E. coli* pol III enzyme with a K_i of 10 μM.[18] It contains a dibromo-substituted aromatic ring which is deeply inserted in sub site 1 and almost superimposes on the peptide L_4 residue of the Pol IV binding peptide. One bromine atom does not form any interaction, while the other forms a halogen bond with β residue T_{172} (d = 3.02 Å and Θ = 133.21°). This latter interaction is similar to that observed for the chlorine atom in the meta position of F_5 in P14.

This specific positioning of halogen-substituted ligands in subsite 1 of the β-clamp contrasts with the wider range of positions occupied by natural amino acids in the same pocket. Indeed, the comparison of different structures of β in complex with various natural peptides (1OK7, 3D1E, 3D1F)[17,18] reveals that, while most of the peptide residues adopt the same overall conformation within the pocket, the position of the last C-terminal residues of the interacting sequence varies in subsite 1. This suggests that no specific interaction is established with a specific β residue, but instead that this hydrophobic interaction, delocalized in all subsite 1, contributes mainly to pasting the peptide onto the β surface.

In conclusion, our structure-based approach allows the design of ligands that bind 2 orders of magnitude more tightly than the natural peptide P1, reaching the 10^{-8} M range, and 4-fold more than the Pol IV enzyme. This increase in affinity relies both on chemical substitutions introduced on the peptide that increase the hydrophobic interactions and on the fact that we retain the bidentate interaction of the ligand in the binding pocket. This interaction mode promotes the modeling of an efficient binding site, possibly through an induced-fit process.

Further designs of high-affinity ligands should also take into account the dynamic nature of the binding site formation. These observations are likely to have major implications on the development of new antibiotic compounds.

EXPERIMENTAL SECTION

Protein Production, Purification, and Characterization. The *E. coli* dnaN gene was cloned into pET15b plasmid (Invitrogen)

dx.doi.org/10.1021/jm200311m |*J. Med. Chem.* 2011, 54, 4627–4637

using standard protocols. The resulting N-tagged protein was expressed in BL21 *E. coli* cells after IPTG induction (0.1 mM) at 28 °C. The β protein fraction was first enriched on a Ni-NTA column, eluted with an histidine step (300 mM), and further purified on a MonoQ column in buffer containing 20 mM Tris HCl pH 7.5, 0.5 mM EDTA, and 10% glycerol, using a gradient from 0 to 0.5 M NaCl. The quality of the protein was assessed by mass spectrometry in denaturing and native conditions (data not shown).

Peptide Synthesis. Peptides P1−P14 were synthesized in Fmoc chemistry by the stepwise solid-phase methodology[28] on a homemade semiautomatic peptide synthesizer.[29] Assembly of the protected peptide chains was carried out on a 100-μmol scale starting from either Fmoc-Leu-Wang resin (peptides P1, P2, P4), Fmoc-Phe-Wang (peptides P3, P5−P10) resin or *o*-chlorotrityl chloride resin (peptide P11−P14). For each coupling step, the reactants were introduced manually as a solution in dry DMF (2.0 mL). N_α-Fmoc amino acids (5.0 equiv) with standard side-chain protecting groups were coupled 2 times by using BOP (5.0 equiv), HOBt (5.0 equiv), and DIEA (10.0 equiv) in dry DMF for 20 min. The washing of the resin as well as Fmoc deprotection (by using a freshly prepared solution of 20% piperidine in DMF) were performed automatically. The coupling and deprotection steps were monitored by the Kaiser test.[30] At the end of the elongation of the peptidic chain, the resin was washed with CH_2Cl_2 and dried with Et_2O. A mixture of TFA/H_2O/TIPS/DTT (8.8:0.5:0.2:0.5; 10.0 mL) was then added to the resin. The mixture was gently shaken for 2.5 h and the resulting solution was flushed through a frit in cold Et_2O. The precipitate was recovered by centrifugation, dissolved in a mixture of AcOH and H_2O and freeze−dried. The crude peptides were finally purified by HPLC (linear gradient, 5−65% B, 30 min) and freeze−dried. All peptides were identified by matrix-assisted laser desorption/ionization mass spectrometry (MALDI-MS), and their homogeneity was assessed by C_{18} RP-HPLC (purity of all peptides determined to be >90%). Analytical data are reported in Supporting Information 1.

Molecular Dynamics. In the present work, we use a protocol[31] based on the MM/PBSA method[32,33] where conformations extracted from molecular dynamics simulations are processed using a simplified description for the solvent to yield an estimate of binding free energy. Individual contributions of each amino acid to the complex formation are estimated, and important energetic amino acid "hot spots" are identified.

Structures. The initial structure for the apo protein was chain A from the PDB file 1OK7,[17] while for the protein and native peptide, it was chains B and C from the same PDB (1OK7). All crystallographic water molecules were retained.

MD Simulations. The CHARMM program,[34] version 32, with the CHARMM 22 all-atom protein-nucleic acid force field[35] was used for the molecular dynamics simulations. Hydrogen atoms were added using the HBUILD facility in the CHARMM program. A sphere of 37 Å containing 6840 water molecules (TIP3) was used to solvate the system. Stochastic boundary conditions were imposed and the calculation was limited to residues 7 Å around the peptide. The SHAKE algorithm was used to constrain hydrogen−heavy atom bond distances, and the simulations were done using Langevin algorithm. A 1 fs time step was used for the molecular dynamics simulation and the simulation time. A 12 Å cutoff was used; the van der Waals nonbonded terms were treated with a SWITCH potential function, whereas the electrostatic terms was evaluated with the SHIFT function.

Free Energy Decomposition of Interactions between the *E. coli* β Clamp and the Different Peptides. To obtain a semiquantitative estimate of the contributions of all amino acids to the binding free energy for the formation of the β clamp-peptide complex, a molecular free energy decomposition scheme based on the Molecular Mechanics/Poisson−Boltzmann Surface Area (MM/PBSA) analysis was performed, following the approach presented by Lafont et al.[31] From this analysis, an estimation of the free energy of binding for molecular complexes can be obtained. Briefly, in the MM/PBSA approach, the free energy is estimated using a standard thermodynamic cycle of the form

$$\begin{array}{ccc} \text{Prot} + \text{Peptide} & \xrightarrow{\Delta G_{assoc}^{gas}} & \text{Prot} : \text{Peptide} \\ \downarrow \Delta G_{solv}^{protein} & & \downarrow \Delta G_{solv}^{peptide} \downarrow \Delta G_{solv}^{complex} \\ \text{Prot} : \text{Peptide} & \xrightarrow{\Delta G_{assoc}^{solution}} & \text{Prot} + \text{Peptide} \end{array}$$

where the binding free energy is calculated according to the equation:

$$\Delta G_{assoc}^{solution} = \Delta E_{MM}^{gas} - T\Delta S_{MM} + \Delta G_{solvation}$$

where ΔE_{MM}^{gas} is the difference in the gas phase energy, ΔS_{MM} is the change in entropy upon complex formation, and $\Delta G_{solvation}$ is the change in solvation free energy. The gas phase energy differences contain terms for the intermolecular electrostatic and van der Waals energies, as well as the equivalent internal energy terms. These terms are based on the CHARMM force field in the present approach. The solvation free energy is divided into two contributions: an electrostatic and a nonpolar contribution. This latter term is approximated by an empirical relationship based on solvent accessible surface area and the electrostatic contribution is calculated here using the Poisson−Boltzmann equation.

Several approximations are introduced in the MM/PBSA method. The first was the neglect of conformational change upon complex formation, which is dictated by the absence of experimental structures for the unbound protein and peptides. To account for the unbound species in the calculations, their respective structures were obtained from the complex generated during the molecular dynamics simulations. With this approximation, there are no changes to the internal energy terms. The second approximation is the neglect of changes in configuration entropy due to binding. Although these simplifications preclude calculations of absolute values of the binding free energies, they have been shown in previous work to be satisfactory in the context of identifying interaction energy "hot spots" in protein−protein and protein−ligand complexes. Similar simplifications have been employed in other studies.[36,31,37] Via this approach, the total binding free energy can be decomposed into individual energetic contributions per residue. Decomposition of the binding free energy to individual amino acid contributions leads to the identification of amino acids that play a dominant role in binding and can contribute to reliable predictions of the role of particular amino acids in stabilizing complexes.

Structure-Based Design of Peptides. From the initial structural and energetic analysis of the RQLVLGL (P1 in Table 1) peptide binding to the β clamp, modification of the sequence appeared potentially interesting in three positions (cf. Figure 1): Q2, L3, and the hydrophobic L5-G6-L7 segment. In order to identify interesting modifications, the programs MCSS[38] and SEED[39] were used to dock small librairies of hydrophobic and polar small ligands (fragments) onto the surface of the β-clamp encompassing the peptide binding site. The protocol incorporated improved scoring functions with solvation corrections.[40,41] From this initial step, it appeared difficult to find replacements for the Q2 side-chain of the peptide that would correctly maintain the intricate hydrogen-bond network at this position (see Figure 3), and therefore, no modification of Q2 was attempted. For the other positions, improving interactions with optimized hydrophobic contacts appeared promising. On the basis of these initial data, a selection of peptides with modified side chains was constructed, docked into the structure, and their interactions with the β clamp evaluated using the MM-PBSA protocol described above. The choice of side-chain replacements was based on the docking data, focusing on commercially available protected amino acids. A force field adapted from CHARMM 22[35] was used for

non-natural amino acids. The most promising candidates were selected for synthesis.

β/Peptide Interaction in Solution: In Vitro Competition Assays. 5′ end radiolabeling, purification, and annealing of synthetic primers were performed as previously described (Wagner et al., 1999). The 30/90 mer synthetic construct was obtained by annealing the 30 mer primer (5′GTAAAACGACGGCCAGTGCCAAGCTTAGTC) with the 90 mer template (5′CCATGATTACGAATTCAGTCATCACCG GCGCCACAGACTAAGC TTGGCACTGGCCGTCGTTTTACAA CGTCGTGACTGGGAAAACCCTGG) to form a double-stranded structure with 5′ and 3′ ssDNA overhangs of 25 and 35 nucleotides, respectively. All replication experiments (10 μL final volume) were carried out in buffer E (40 mM HEPES pH 7.5, 80 mM potassium glutamate, 160 μg/mL BSA, 16% glycerol, 0.016% NP40, 8 mM DTT). The 30/90 mer duplex (1 nM final concentration) was first incubated with single strand binding protein (SSB; Sigma; 90 nM final concentration) in the presence of ATP (200 μM) and $MgCl_2$ (7.5 mM) at 37 °C for 10 min. γ complex (1 nM final concentration) (a generous gift of Dr. Charles S. McHenry, University of Colorado, Denver, CO) and β clamp (5 nM as dimer final concentration) were added at that stage and incubation was carried out at 37 °C for 10 min. Then, 7 μL of the mixture was added to 1 μL of either DMSO or 1 μL of peptide solution (as specified), incubated 5 min at room temperature and further 2 h at 4 °C. One microliter of PolIV was then added (1.5 nM final concentration), incubated 5 min at room temperature, and finally, the whole reaction was mixed with 1 μL of a dNTPs solution (200 μM each dNTP final concentration) and allowed to react for 1 min at room temperature. Reactions were quenched by the addition of 20 μL of 95% formamide/dye solution containing 7.5 mM EDTA, heat-denatured, and analyzed by chromatography on 12% denaturing polyacrylamide gels. Radiolabeled products were visualized and quantified using a Personal Molecular Imager Fx and the Quantity One software (Bio-Rad).

SPR Assays. SPR experiments were performed on a Biacore 3000 at 25 °C. The association constant (K_A) of β with the natural C-terminal heptamer (P1, Table 1) of the DNA polymerase IV of *E. coli* were determined as follows: the β protein (0.125 μM to 2 μM) was injected on the immobilized P1 peptide at a flow rate of 50 $\mu L.min^{-1}$. After subtraction of the background response, the data were fit to the 1:1 Langmuir model using BIAevaluation (Biacore). The inhibition of the P1-β interaction by peptides P2 to P14 (Table 1) was used to measure their affinity to β and was assessed according to the following procedure: complexes of β (0.25 μM) with various concentrations of challenging peptides (1.5 nM to 100 μM) were formed and injected on a chip loaded with the P1 peptide. IC_{50} values for each challenging peptide were determined by plotting the concentration of peptide against the percentage of binding inhibition. The IC_{50} value of each peptide was used to calculate K_i ($K_i = (1 + K_A[\beta])/IC_{50}$) which measures the affinity of the challenging peptide for β in the competition assay, and ΔG was derived from K_i ($\Delta G = -RT \ln K_i$).

Isothermal Titration Calorimetry. ITC was performed by using a ITC200 microcalorimeter from MicroCal. Peptides (400 μM) were titrated in sequential injections (2 μL each) into a β solution (300 μL, 20 or 30 μM) at 25 °C. Data were corrected from control experiments where peptides were injected in buffer solution (Hepes 10 mM pH 7.4, NaCl 0.15 M, EDTA 3 mM, P20 0.005%). Data analysis was performed with *Origin 7.0* software.

Crystallogenesis, Data Collection, and Processing. Crystallization experiments were essentially conducted as described previously.[17] Crystals of P12-β complexes were grown in capillaries in the presence of 0.2% of agarose.[42] Crystallization buffer contained 100 mM $CaCl_2$, 100 mM MES pH 6.0, and 30% PEG 400. Cryoprotection was performed by soaking crystals in the same buffer supplemented with 20% glycerol. Cryoprotected crystals were frozen in liquid ethane and X-ray diffraction data were collected at 100 K at beamline X06SA at the Swiss Light Source (Villigen PSI, Switzerland) and beamlines ID29 and ID14−4 at ESRF (Grenoble, France). Diffraction images were processed with XDS, XSCALE, and XDSCONV.[43] The structures were solved by molecular replacement with MOLREP,[44] using the known beta structure as a search model PDB ID 1OK7.[17] Alternate rounds of rebuilding and refinement, including noncrystallographic symmetry restraints, were carried out with PHENIX,[45] COOT,[46] and CNS.[47] Model statistics were obtained with Molprobity.[48] Molecular visualizations and structures illustrations were performed using PyMOL.[49] Data processing and refinement statistics are summarized in Table 2.

■ ASSOCIATED CONTENT

Supporting Information. Analytical data on the peptides, statistics and crystallographic informations, graphical analysis of the biochemical analysis, details on ITC experiments, and a movie illustrating the dynamic of the binding pocket upon ligand interaction. This material is available free of charge via the Internet at http://pubs.acs.org.

■ AUTHOR INFORMATION

Corresponding Author

*E-mail: d.burnouf@ibmc.u-strasbg.fr; phone: 33 3 88 417 002; fax: 33 3 88 602 218.

Author Contributions

■These authors equally contributed to the work.

Author Contributions

△These authors equally initiated and conducted the work.

■ ACKNOWLEDGMENT

Dr. Guillaume Bec and Séverine Freisz for collecting data at ESRF. Dr. Johan Hoebeke for helping to set up the SPR experiments, Nicolas Ambert who participated in the initial phase of this project and Dr Y.Timsit for helpful discussions and insights in pictures drawing.

■ ABBREVIATIONS

Ac, acetyl group; Cha, β-cyclohexyl-L-alanyl; hCha, L-homoCha; Hol, L-homoleucyl; NptGly, neopentylglycyl; *p*MePhe, 4-methyl-L-phenylalanyl; pClPhe, 4-chloro-L-phenylalanyl; *p*BrPhe, 4-bromo-L-phenylalanyl; (3,4-di-Cl)Phe, 3,4-dichloro-L-phenylalanyl; PCNA, proliferating cell nuclear antigen; SPR, surface plasmon resonance; ITC, isothermal titration calorimetry; β, replicase processivity factor; V_M, Matthew's number; rmsd, root-mean-square deviation; MCSS, multiple copy simultaneous search; SEED, solvation energy for exhaustive docking; IC_{50}, half-maximum inhibitory concentration; IPTG, isopropyl β-D-1-thiogalactopyranoside; Ni-NTA, nickel-nitrilotriacetic acid; MM-PBSA, molecular mechanics/Poisson−Boltzmann surface area; SS-DNA, single-stranded DNA; SSB, single-stranded binding protein; ESRF, European synchrotron radiation facility

■ REFERENCES

(1) Kong, X. P.; Onrust, R.; O'Donnell, M.; Kuriyan, J. Three-dimensional structure of the beta subunit of E. coli DNA polymerase III holoenzyme: a sliding DNA clamp. *Cell* **1992**, *69*, 425–437.

(2) Gulbis, J. M.; Kelman, Z.; Hurwitz, J.; O'Donnell, M.; Kuriyan, J. Structure of the C-terminal region of p21(WAF1/CIP1) complexed with human PCNA. *Cell* **1996**, *87*, 297–306.

(3) Shamoo, Y.; Steitz, T. A. Building a replisome from interacting pieces: sliding clamp complexed to a peptide from DNA polymerase and a polymerase editing complex. *Cell* **1999**, *99*, 155–166.
(4) Matsumiya, S.; Ishino, Y.; Morikawa, K. Crystal structure of an archaeal DNA sliding clamp: proliferating cell nuclear antigen from Pyrococcus furiosus. *Protein Sci.* **2001**, *10*, 17–23.
(5) Johnson, A.; O'Donnell, M. Cellular DNA replicases: components and dynamics at the replication fork. *Annu. Rev. Biochem.* **2005**, *74*, 283–315.
(6) Fuchs, R. P.; Fujii, S. Translesion synthesis in Escherichia coli: lessons from the NarI mutation hot spot. *DNA Repair (Amst.)* **2007**, *6*, 1032–1041.
(7) Prakash, S.; Johnson, R. E.; Prakash, L. Eukaryotic translesion synthesis DNA polymerases: specificity of structure and function. *Annu. Rev. Biochem.* **2005**, *74*, 317–353.
(8) Kleczkowska, H. E.; Marra, G.; Lettieri, T.; Jiricny, J. hMSH3 and hMSH6 interact with PCNA and colocalize with it to replication foci. *Genes Dev.* **2001**, *15*, 724–736.
(9) Lopez de Saro, F. J.; Marinus, M. G.; Modrich, P.; O'Donnell, M. The beta sliding clamp binds to multiple sites within MutL and MutS. *J. Biol. Chem.* **2006**, *281*, 14340–14349.
(10) Dalrymple, B. P.; Kongsuwan, K.; Wijffels, G.; Dixon, N. E.; Jennings, P. A. A universal protein-protein interaction motif in the eubacterial DNA replication and repair systems. *Proc. Natl. Acad. Sci. U.S.A.* **2001**, *98*, 11627–11632.
(11) Wagner, J.; Fujii, S.; Gruz, P.; Nohmi, T.; Fuchs, R. P. The beta clamp targets DNA polymerase IV to DNA and strongly increases its processivity. *EMBO Rep.* **2000**, *1*, 484–488.
(12) Becherel, O. J.; Fuchs, R. P.; Wagner, J. Pivotal role of the beta-clamp in translesion DNA synthesis and mutagenesis in E. coli cells. *DNA Repair (Amst.)* **2002**, *1*, 703–708.
(13) Lenne-Samuel, N.; Wagner, J.; Etienne, H.; Fuchs, R. P. The processivity factor beta controls DNA polymerase IV traffic during spontaneous mutagenesis and translesion synthesis in vivo. *EMBO Rep.* **2002**, *3*, 45–49.
(14) Heltzel, J. M.; Maul, R. W.; Scouten Ponticelli, S. K.; Sutton, M. D. A model for DNA polymerase switching involving a single cleft and the rim of the sliding clamp. *Proc. Natl. Acad. Sci. U.S.A.* **2009**, *106*, 12664–12669.
(15) Jeruzalmi, D.; Yurieva, O.; Zhao, Y.; Young, M.; Stewart, J.; Hingorani, M.; O'Donnell, M.; Kuriyan, J. Mechanism of processivity clamp opening by the delta subunit wrench of the clamp loader complex of E. coli DNA polymerase III. *Cell* **2001**, *106*, 417–428.
(16) Bunting, K. A.; Roe, S. M.; Pearl, L. H. Structural basis for recruitment of translesion DNA polymerase Pol IV/DinB to the beta-clamp. *Embo J.* **2003**, *22*, 5883–5892.
(17) Burnouf, D. Y.; Olieric, V.; Wagner, J.; Fujii, S.; Reinbolt, J.; Fuchs, R. P.; Dumas, P. Structural and biochemical analysis of sliding clamp/ligand interactions suggest a competition between replicative and translesion DNA polymerases. *J. Mol. Biol.* **2004**, *335*, 1187–1197.
(18) Georgescu, R. E.; Yurieva, O.; Kim, S. S.; Kuriyan, J.; Kong, X. P.; O'Donnell, M. Structure of a small-molecule inhibitor of a DNA polymerase sliding clamp. *Proc. Natl. Acad. Sci. U.S.A.* **2008**, *105*, 11116–11121.
(19) Wagner, J.; Etienne, H.; Fuchs, R. P.; Cordonnier, A.; Burnouf, D. Distinct beta-clamp interactions govern the activities of the Y family PolIV DNA polymerase. *Mol. Microbiol.* **2009**, *74*, 1143–1151.
(20) Auffinger, P.; Hays, F. A.; Westhof, E.; Ho, P. S. Halogen bonds in biological molecules. *Proc. Natl. Acad. Sci. U.S.A.* **2004**, *101*, 16789–16794.
(21) Rinnenthal, J.; Klinkert, B.; Narberhaus, F.; Schwalbe, H. Direct observation of the temperature-induced melting process of the Salmonella fourU RNA thermometer at base-pair resolution. *Nucleic Acids Res.* **2010**, *38*, 3834–3847.
(22) Strazewski, P. Thermodynamic correlation analysis: hydration and perturbation sensitivity of RNA secondary structures. *J. Am. Chem. Soc.* **2002**, *124*, 3546–3554.
(23) Ackroyd, P. C.; Cleary, J.; Glick, G. D. Thermodynamic basis for sequence-specific recognition of ssDNA by an autoantibody. *Biochemistry* **2001**, *40*, 2911–2922.
(24) Voth, A. R.; Ho, P. S. The role of halogen bonding in inhibitor recognition and binding by protein kinases. *Curr. Top. Med. Chem.* **2007**, *7*, 1336–1348.
(25) Camacho, C. J.; Kimura, S. R.; DeLisi, C.; Vajda, S. Kinetics of desolvation-mediated protein-protein binding. *Biophys. J.* **2000**, *78*, 1094–1105.
(26) Vijayakumar, S.; Chapados, B. R.; Schmidt, K. H.; Kolodner, R. D.; Tainer, J. A.; Tomkinson, A. E. The C-terminal domain of yeast PCNA is required for physical and functional interactions with Cdc9 DNA ligase. *Nucleic Acids Res.* **2007**, *35*, 1624–1637.
(27) Arkin, M. R.; Randal, M.; DeLano, W. L.; Hyde, J.; Luong, T. N.; Oslob, J. D.; Raphael, D. R.; Taylor, L.; Wang, J.; McDowell, R. S.; Wells, J. A.; Braisted, A. C. Binding of small molecules to an adaptive protein-protein interface. *Proc. Natl. Acad. Sci. U.S.A.* **2003**, *100*, 1603–1608.
(28) Goodman, M.; Felix, A.; Moroder, L.; Toniolo, C. H.-W. *Synthesis of Peptides and Peptidomimetics*; Thieme: Stuttgart, NY; Vol. E 22a—e.
(29) Neimark, J.; Briand, J. P. Development of a fully automated multichannel peptide synthesizer with integrated TFA cleavage capability. *Pept. Res.* **1993**, *6*, 219–228.
(30) Kaiser, E.; Colescott, R. L.; Bossinger, C. D.; Cook, P. I. Color test for detection of free terminal amino groups in the solid-phase synthesis of peptides. *Anal. Biochem.* **1970**, *34*, 595–598.
(31) Lafont, V.; Schaefer, M.; Stote, R.; Altschuh, D.; Dejaegere, A. Protein-protein recognition and interaction hot spots in an antigen-antibody complex: free energy decomposition identifies "efficient amino acids. *Proteins: Struct. Funct. Bioinformatics* **2007**, *67*, 418–434.
(32) Kollman, P. A.; Massova, I.; Reyes, C.; Kuhn, B.; Huo, S.; Chong, L.; Lee, M.; Lee, T.; Duan, Y.; Wang, W.; Donini, O.; Cieplak, P.; Srinivasan, J.; Case, D. A. Calculating structures and free energies of complex molecules: combining molecular mechanics and continuum models. *Acc. Chem. Res.* **2000**, *33*, 889–897.
(33) Gohlke, H.; Kiel, C.; Case, D. A. Insights into protein-protein binding by binding free energy calculation and free energy decomposition for the Ras-Raf and Ras-RalGDS complexes. *J. Mol. Biol.* **2003**, *330*, 891–913.
(34) Brooks, B. R.; Bruccoleri, R. E.; Olafson, B. D.; States, D. J.; Swaminathan, S.; M., K. CHARMM: A program for macromolecular energy minimization and dynamics calculations. *J. Comput. Chem.* **1983**, *4*, 187–217.
(35) MacKerell, A. D.; Bashford, D.; Bellott, M.; Dunbrack, R. L.; Evanseck, J. D.; Field, M. J.; Fischer, S.; Gao, J.; Guo, H.; Ha, S.; Joseph-McCarthy, D.; Kuchnir, L.; Kuczera, K.; Lau, F. T. K.; Mattos, C.; Michnick, S.; Ngo, T.; Nguyen, D. T.; Prodhom, B.; Reiher, W. E.; Roux, B.; Schlenkrich, M.; Smith, J. C.; Stote, R.; Straub, J.; Watanabe, M.; Wiorkiewicz-Kuczera, J.; Yin, D.; Karplus, M. All-atom empirical potential for molecular modeling and dynamics studies of proteins. *J. Phys. Chem. B* **1998**, *102*, 3586–3616.
(36) Hendsch, Z. S.; Tidor, B. Electrostatic interactions in the GCN4 leucine zipper: substantial contributions arise from intramolecular interactions enhanced on binding. *Protein Sci.* **1999**, *8*, 1381–1392.
(37) Gouda, H.; Kuntz, I. D.; Case, D. A.; Kollman, P. A. Free energy calculations for theophylline binding to an RNA aptamer: Comparison of MM-PBSA and thermodynamic integration methods. *Biopolymers* **2003**, *68*, 16–34.
(38) Miranker, A.; Karplus, M. Functionality maps of binding sites: a multiple copy simultaneous search method. *Proteins* **1991**, *11*, 29–34.
(39) Majeux, N.; Scarsi, M.; Apostolakis, J.; Ehrhardt, C.; Caflisch, A. Exhaustive docking of molecular fragments with electrostatic solvation. *Proteins* **1999**, *37*, 88–105.
(40) Sirockin, F.; Sich, C.; Improta, S.; Schaefer, M.; Saudek, V.; Froloff, N.; Karplus, M.; Dejaegere, A. Structure activity relationship by NMR and by computer: a comparative study. *J. Am. Chem. Soc.* **2002**, *124*, 11073–11084.
(41) Majeux, N.; Scarsi, M.; Caflisch, A. Efficient electrostatic solvation model for protein-fragment docking. *Proteins* **2001**, *42*, 256–268.
(42) Biertumpfel, C.; Basquin, J.; Suck, D.; Sauter, C. Crystallization of biological macromolecules using agarose gel. *Acta Crystallogr., Sect. D* **2002**, *58*, 1657–1659.

(43) Kabsch, W. Automatic processing of rotation diffraction data from crystals of initially unknown symmetry and cell constants. *J. Appl. Crystallogr.* **1993**, *26*, 795–800.

(44) Collaborative Computational Project, N., The CCP4 suite: programs for protein crystallography. *Acta Crystallogr., Sect. D Biol. Crystallogr. D50* **1994**, 760−763.

(45) Adams, P. D.; Grosse-Kunstleve, R. W.; Hung, L. W.; Loerger, T. R.; McCoy, A. J.; et al. PHENIX: building new software for automated crystallographic structure determination. *Acta Crystallogr., Sect. D Biol. Crystallogr. D50* **2002**, *58*, 1948–1954.

(46) Emsley, P.; Cowtan, K. Coot: model-building tools for molecular graphics. *Acta Crystallogr., Sect. D Biol. Crystallogr. D50* **2004**, *60*, 2126–2132.

(47) Brünger, A. T.; Adams, P. D.; Clore, G. M.; Delano, W. L.; Gros, P.; Grosse-Kuntsleve, R. V.; et al. Crystallography and NMR system: a new software suite for macromolecular structure determination. *Acta Crystallogr., Sect. D* **1998**, *54*, 905–921.

(48) Chen, V. B.; Arendall, W. B. r.; Headd, J. J.; Keedy, D. A.; Immormino, R. M.; Kapral, G. J.; Murray, L. W.; Richardson, J. S. R.; D., C. MolProbity: all-atom structure validation for macromolecular crystallography. *Acta Crystallogr., Sect. D* **2010**, *66*, 12–21.

(49) DeLano, W. L. *The PyMOL Molecular Graphics System*; DeLano Scientific LLC: Palo Alto, CA, USA, 2008.